Nanoscale

Understanding the Rod-to-Tube Transformation of Self-Assembled Ascorbyl Dipalmitate Lipid Nanoparticles Stabilized with PEGylated Lipids

Journal:	*Nanoscale*
Manuscript ID	NR-ART-09-2022-004987.R1
Article Type:	Paper
Date Submitted by the Author:	01-Dec-2022
Complete List of Authors:	Ziqiao, Chen ; Chiba University Higashi, Kenjirou; Chiba University, Graduate School of Pharmaceutical Sciences; Chiba University Shigehisa, Yuki ; Chiba University Ueda, Keisuke ; Chiba University Yamamoto, Keiji; Chiba University Moribe, Kunikazu; Chiba University,

Understanding the Rod-to-Tube Transformation of Self-Assembled Ascorbyl Dipalmitate Lipid Nanoparticles Stabilized with PEGylated Lipids

*Ziqiao Chen†, Kenjirou Higashi†, Yuki Shigehisa, Keisuke Ueda, Keiji Yamamoto, Kunikazu Moribe**

Graduate School of Pharmaceutical Sciences, Chiba University, 1-8-1 Inohana, Chuo-ku, Chiba 260-8675, Japan.

† These authors contributed equally to this manuscript.

* Corresponding author. Tel.: +81-43-226-2865; Fax: +81-43-226-2867.

E-mail: moribe@faculty.chiba-u.jp (K. Moribe).

ABSTRACT

We previously established a nanoparticle-based drug delivery system (DDS) for high-dose ascorbic acid therapy by self-assembly of a lipid-modified ascorbic acid derivative, L-ascorbyl 2,6-dipalmitate (ASC-DP). The particles' morphology should be modified for effective DDSs. Here, we modulated the morphology of self-assembled ASC-DP nanoparticles using two different PEGylated lipids, distearoylphosphatidylethanolamine-polyethylene glycol (DSPE-PEG) and cholesterol-polyethylene glycol (Chol-PEG), with various PEG molecular weights. At the preparation molar ratio of 10:1 (ASC-DP/PEGylated lipid), rod-like nanoparticles

emerged in the ASC-DP/DSPE-PEG system, whereas the ASC-DP/Chol-PEG system yielded tube-like nanoparticles. The internal structures of both rod-like ASC-DP/DSPE-PEG and tube-like ASC-DP/Chol-PEG nanoparticles were similar to that of repeated ASC-DP bilayers. The particles' surfaces featured PEGylated lipids, which stabilized the structure and dispersion of the nanoparticles. For both systems, the particle size increased slightly with increasing the PEGylated liquid's PEG molecular weight. Increasing the PEG molecular weight decreased the inner tunnel size of tube-like ASC-DP/Chol-PEG nanoparticles. A mechanism has been proposed for the rod-to-tube transformation. Surface-layer free-energy changes owing to the mixing of multiple lipids and PEG chain repulsion are thought to underlie the inner tunnels' formation. The rod-to-tube morphology of self-assembled ASC-DP nanoparticles can be modulated by controlling the PEGylated lipids' structure, including the lipid species and the PEG chain length.

KEYWORDS: Morphology control, Self-assembly, PEGylated lipid, Cylindrical nanoparticles, Organic nanotube, High-dose ascorbic acid therapy

INTRODUCTION

Ascorbic acid, also known as ascorbate and vitamin C, is widely used in nutrition,[1] cosmetics,[2] and foods,[3] owing to its excellent antioxidant effect. Ascorbic acid has been shown to have antitumor activity and has garnered significant attention as a novel complementary therapy for cancers.[4, 5] Parenteral administration (i.v. injection) of ascorbic acid selectively damages tumor cells without adversely affecting normal cells.[6] However, to achieve the antitumor effect of ascorbic acid, high-dose administration is required.[4, 5] The pro-oxidant

property of ascorbic acid at a high dose has been suggested to account for its antitumor activity.[7] Yun et al.[8] demonstrated that cancer cells increasingly take up the oxidized form of ascorbic acid when exposed to high levels of ascorbic acid, leading to oxidative stress and eventually cell death. In addition, ascorbic acid is easily decomposed by light, heat, and metal ions. Therefore, effective and stable drug delivery systems (DDSs) are desirable for delivering ascorbic acid to tumors.

Nanoparticles have been widely employed as DDSs for targeted cancer therapy.[9, 10] In recent years, nanoparticle-based ascorbic acid delivery has attracted attention.[7] Compared to molecular ascorbic acid, ascorbic acid in the nanoparticle form is more stable and easier to deliver into the cell by endocytosis. Chakraborty et al.[11] formulated ascorbic acid as nanoparticles and reported that the nanoparticle form of ascorbic acid provides chemical stability under physiological conditions and offers glucose-responsive efficient delivery of ascorbic acid into cells. They also demonstrated that the nanoparticle form of ascorbic acid induces cell death by generating oxidative stress at a high dose. Nanoparticles for cancer therapy function by passively accumulating in tumor tissue, utilizing the enhanced permeability and retention (EPR) effect.[12, 13] The particle sizes and shapes significantly affect their biodistribution. For instance, smaller nanoparticles (< 6 nm) are quickly eliminated from the body by renal excretion, while nanoparticles with sizes above 200 nm tend to accumulate in the spleen and liver.[14] Silicon-based particles with spherical, discoidal, quasi-hemispherical, and cylindrical shapes tend to accumulate in different tissues after i.v. administration.[15] Rod-shaped polystyrene nanoparticles carrying antibodies enhance the specific uptake to target cells, compared with spherical particles.[16] Hence, the nanoparticles' morphological aspects, including their size and geometric shape, should be considered for their applications.

Controlling the morphology of nanoparticles is a challenging task. One-dimensional

nanostructures (such as nanorods and nanotubes) are commonly fabricated by the self-assembly of constituent molecules.[17-19] The constituent molecules self-associate into architectures, owing to the thermodynamic minimization of free energy.[20] Specifically, molecules that contain lipid acyl chains can organize into mono-/multi-layers with long-range order, yielding cylindrical structures.[21-24] The morphology of such self-assembled lipid cylinders can be controlled by modulating the lipid structure.[23, 24] In addition, PEGylated lipids have been used for modifying lipid assemblies such as liposomes, solid lipid nanoparticles, and nanostructured lipid carriers.[25, 26] Polyethylene glycol (PEG) chains form hydration shells around nanoparticles, increasing their stability and dispersity.[27, 28] This PEG-based surface modification increases the blood circulation time of the nanoparticles after their i.v. administration.[29, 30] The pharmacokinetics and biodistribution of such PEG-modified nanoparticles are affected by the PEG surface conformation, which predominantly depends on the PEG molecular weight and surface density.[31-34] For instance, a densely packed PEG "brush" conformation is superior to a collapsed "mushroom" conformation for stealth nanoparticles with weak nanoparticle–cell interactions.[33]

In our previous study, we used L-ascorbyl 2,6-dipalmitate (ASC-DP) to establish a nanoparticle-based DDS for high-dose ascorbic acid delivery.[35-37] ASC-DP is a lipid-modified ascorbic acid derivative that increases the stability of ascorbic acid. ASC-DP caused cytotoxicity against the A549, LC-AI, and MKN45 cell lines after 3 and 6 h of exposure, whereas significant cell toxicity was not observed when employing healthy cells like fibroblasts.[36] ASC-DP molecules self-assembled into nanoparticles with a PEGylated lipid, distearoylphosphatidylethanolamine-polyethylene glycol 2000 (DSPE-PEG2000). ASC-DP/DSPE-PEG2000 nanoparticles exhibited unique shapes, including disks, tubes, and rods, depending on the initial molar ratio of ASC-DP and DSPE-PEG2000 used in the preparation

process (Figure 1).[35, 36] The nanostructures of these particles were thoroughly examined using small-angle X-ray scattering (SAXS).[35] Uniform rod-like nanoparticles (diameter, approximately 100 nm; length, 300 nm) were obtained at the preparation molar ratio of 10:1. Although rod-like nanoparticles exhibit a high ASC-DP loading of 94.1% (w/w), tube-like nanoparticles are more promising as DDSs for targeted cancer therapy, because the inner tunnel space can serve as a potential platform for loading other antitumor drugs for combination therapy. Many types of self-assembled organic nanotubes have been developed for drug delivery.[38, 39] Unfortunately, tube-like nanoparticles prepared at the medium preparation ratio of ASC-DP/DSPE-PEG2000 in our previous study were highly polydisperse and unexpectedly mixed with disk- and rod-like nanoparticles. Therefore, in the present study, we prepared uniform tube-like nanoparticles and established a strategy for modulating the rod-to-tube nanoparticle morphology by evaluating the effects of PEGylated lipid species and PEG chain length on the formation of nanoparticles. In addition to DSPE-PEG, another PEGylated lipid, cholesterol-PEG (Chol-PEG), was used. It is widely known that the addition of cholesterol to the lipid bilayer alters the bilayer stability and in vivo performance.[40, 41] Similar effects have been reported for Chol-PEG.[42]

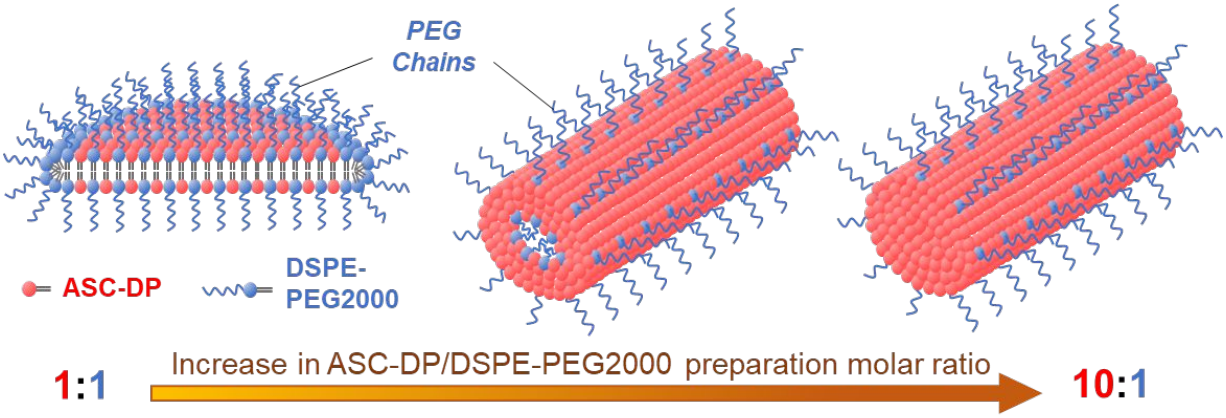

Figure 1. Schematic of the proposed structures of ASC-DP nanoparticles with different

morphologies, prepared using different molar ratios of ASC-DP/DSPE-PEG2000. Reconstructed from reference 35.

MATERIALS AND METHODS

Materials

ASC-DP was acquired from Tokyo Chemical Industry Co., Ltd. (Tokyo, Japan). DSPE-PEG750 was purchased from Avanti Polar Lipids, Inc. (Alabama, USA). DSPE-PEG2000 (SUNBRIGHT® DSPE-020CN), DSPE-PEG5000 (SUNBRIGHT® DSPE-050CN), Chol-PEG600 (SUNBRIGHT® CS-010), Chol-PEG1500 (SUNBRIGHT® CS-020), and Chol-PEG4600 (SUNBRIGHT® CS-050) were purchased from NOF Corp. (Tokyo, Japan). Purified water was obtained using a Milli-Q system (Millipore SAS, France). All other chemicals were of reagent grade and were used without further purification. The chemical structures and molecular weights (MWs) of ASC-DP, DSPE-PEG, and Chol-PEG are shown in Figure 2.

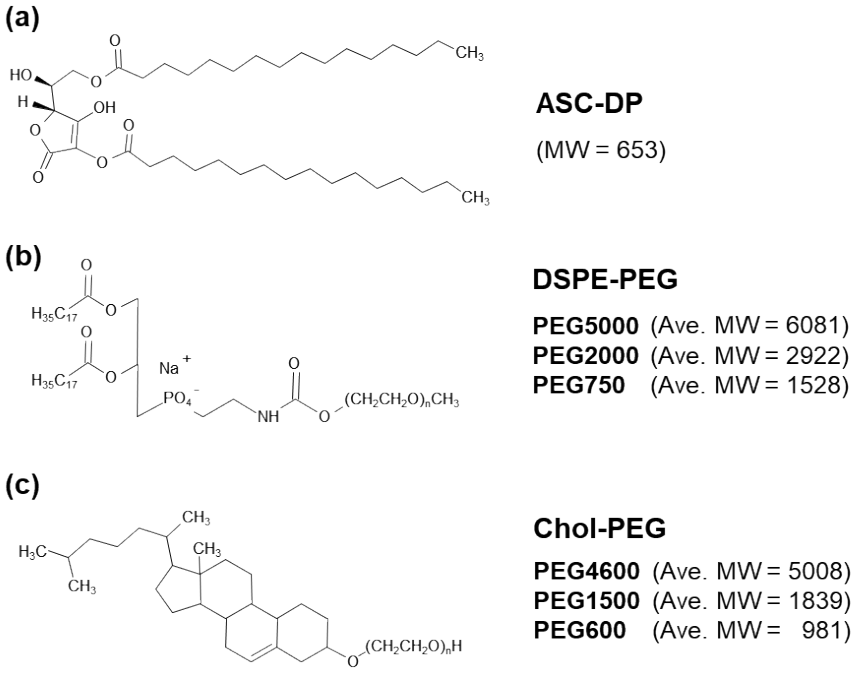

Figure 2. Chemical structures and molecular weights of (a) ASC-DP, (b) DSPE-PEG, and (c) Chol-PEG used in this study.

Preparation of nanoparticles

ASC-DP and PEGylated lipids with designed molar ratios were dissolved in chloroform. Subsequently, the solvent was removed by rotary evaporation using a Büchi EL 131 Rotavapor (Flawil, Switzerland) at 60 ºC, yielding thin films. The films were then dried at room temperature under reduced pressure. The dried films were hydrated with purified water at the ASC-DP concentration of 2 mM, and sonicated at 60 ºC for 3 min using a bath sonicator (Bransonic Ultrasonic Cleaners 1510J-DTH, Branson Ultrasonic Corp., USA) to obtain suspensions containing the nanoparticles.

Particle size evaluation by dynamic light scattering (DLS)

The particle size distribution and mean volume diameter (MV) of the nanoparticles were determined by DLS using a MICROTRAC 9340-UPA-UT151 ultrafine particle analyzer (UPA®) (MicrotracBEL Corp.; measurement range, 0.0008−6.5 μm).

Field-emission transmission electron microscopy (FE-TEM) measurements

FE-TEM measurements were conducted using a JEM-2100F instrument (JEOL Ltd., Tokyo, Japan) at an accelerating voltage of 120 kV. A carbon-coated 200-mesh copper grid (Excel support film, Nisshin EM Co., Japan) was hydrophilized using a hydrophilic treatment device HDT-400 (JEOL Ltd., Tokyo, Japan) for 40 s. The suspension containing the nanoparticles was dropped onto the grid and allowed to stand for 1 min. The grid was then blotted with filter paper to remove the excess sample, followed by negative staining with 2% phosphotungstic

acid solution (pH = 7.4) for 1 min. The grid was dried in a desiccator for 1 d before FE-TEM measurements.

^{1}H nuclear magnetic resonance (NMR) measurements

The micelle-free nanoparticle suspensions (Supporting Information S1) were freeze-dried using an Eyela FDU-2100 freeze-dryer (Tokyo Rikakikai Co. Ltd., Japan) to obtain dried nanoparticles for ^{1}H NMR measurements, to quantify and characterize the PEG chains on the nanoparticles' surface. The dried nanoparticles were dissolved in deuterated methanol (CD_3OD) or dispersed in heavy water (D_2O) as the NMR samples. Trimethylsilylpropanoic acid (TSP, 0.0 ppm) of 1 mM was used as the internal standard. The concentration of detectable PEG was calculated by comparing the ratio of the integral value of the PEG peak to that of the TSP peak using a calibration curve, which was constructed using standard solutions.

To determine the composition of the nanoparticles, the precipitates collected after centrifugation of the freshly prepared nanoparticle suspensions at 15,000 rpm for 40 min were dissolved in deuterated chloroform ($CDCl_3$) and analyzed using ^{1}H NMR spectroscopy (Supporting Information S2). Chemical shifts were referenced to the internal signal of 1 mM 1,4-bis(trimethylsilyl)benzene at 0.23 ppm. The molar ratios of the ASC-DP/PEGylated lipids in the nanoparticles were calculated based on the determined concentrations of each component. The ratio of the integral value of the alkyl methylene peak (1.25 ppm) and PEG methylene peak (3.63 ppm) against that of the internal signal was utilized for determining the concentrations of ASC-DP and PEGylated lipid, respectively. The concentrations were calculated using a calibration curve constructed using standard solutions.

All ^{1}H NMR spectra were obtained using a JNM-ECX400 NMR spectrometer (JEOL Ltd.,

Tokyo, Japan) with a magnetic field of 9.39 T, using 5 mm NMR tubes. The ^{1}H NMR spectra were recorded at 25 °C, at a spinning rate of 15 Hz, relaxation delay of 15 s, and scan of 64 accumulations.

X-ray diffraction (XRD) measurements

The XRD patterns of the precipitates after centrifugation, as mentioned above, were recorded using a MiniFlex II desktop X-ray diffractometer (Rigaku Co., Ltd., Tokyo, Japan). The X-ray generator was operated at 30 kV and 15 mA using a Cu-Kα radiation source (λ = 1.5418 Å). The 2θ angular range of 2−35° was scanned at a rate of 4°/min, at room temperature.

RESULTS AND DISCUSSION

Formation of nanoparticles at different preparation molar ratios of the ASC-DP/PEGylated lipid

DSPE-PEG and Chol-PEG were used as PEGylated lipids to modify the morphology of ASC-DP nanoparticles. According to our previous study,[35] the size of the obtained ASC-DP nanoparticles depends on the initial molar ratio of the ASC-DP/PEGylated lipid used in the preparation process. Hence, PEGylated lipids with mid-sized PEG chains (DSPE-PEG2000 and Chol-PEG1500) were first used, to evaluate the formation of ASC-DP nanoparticles at different preparation molar ratios of the ASC-DP/PEGylated lipid. The ASC-DP/DSPE-PEG2000 system exhibited a maximal particle size of approximately 420 nm at the preparation molar ratio of 3:1 (Figure 3a, blue circles) because the morphology of the nanoparticles changed progressively from disk, tube, long-rod, to short-rod with increasing molar ratio (Figure 1).[35] For the ASC-DP/Chol-PEG1500 system (Figure 3a, green squares), a similar trend was observed: the particle size exceeded 800 nm at the preparation molar ratio of 1:1, followed by a progressive decrease with a further increase in the molar ratio. At the preparation molar ratio of 10:1, both systems yielded nanoparticles with sizes smaller than 250 nm (Figure 3a, arrows). The ASC-DP/DSPE-PEG2000 nanoparticles at the preparation molar ratio of 10:1 were rod-shaped, whereas the ASC-DP/Chol-PEG1500 nanoparticles prepared at the same molar ratio were tube-shaped, with an inner tunnel space (Figure 3b, c). Both the rod-like and tube-like nanoparticles were 200 to 300 nm long, and their diameter was approximately 100 nm. The estimated diameter of the inner tunnel space for the tube-like ASC-DP/Chol-PEG1500 nanoparticles was approximately 10 nm. The FE-TEM images displaying circle structures, which reflect the vertical positions of the nanoparticles, further demonstrated the cylindrical

structures with and without an inner tunnel for the rod-like ASC-DP/DSPE-PEG2000 and tube-like ASC-DP/Chol-PEG1500 nanoparticles, respectively (Supporting Information S3). The concentric circle with lower image contrast in the FE-TEM image of tube-like ASC-DP/Chol-PEG1500 nanoparticles had a diameter of approximately 10 nm (Supporting Information S3, Figure S3b), well agreed with the tunnel size observed in Figure 3c. After the removal of free PEGylated lipid micelles (Supporting Information S1), the particle size distributions for the both systems, as determined by DLS, became unimodal, with average particle sizes of 231 and 198 nm, respectively (Figure 3d, e).

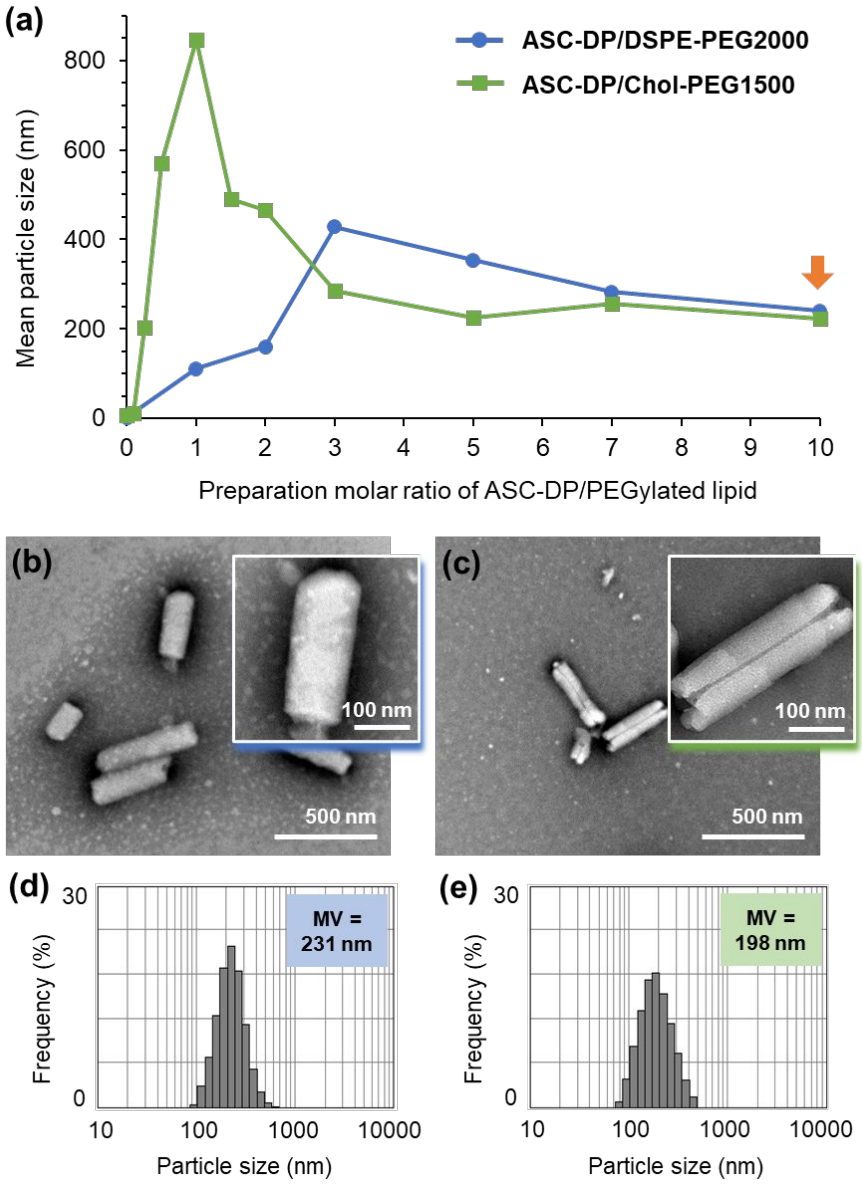

Figure 3. (a) Mean particle sizes, for ASC-DP/DSPE-PEG2000 and ASC-DP/Chol-PEG1500 nanoparticles prepared at various initial molar ratios. (b, c) FE-TEM images and (d, e) particle size distribution patterns of (b, d) ASC-DP/DSPE-PEG2000 and (c, e) ASC-DP/Chol-PEG1500 nanoparticles prepared at the molar ratio of 10:1.

Investigation of PEG chains on the nanoparticles' surfaces

To quantify and characterize the PEG chains on the surfaces of the rod-like ASC-DP/DSPE-

PEG2000 and tube-like ASC-DP/Chol-PEG1500 nanoparticles, ^{1}H NMR spectroscopy was employed. ^{1}H NMR spectroscopy is a powerful tool for quantifying the components of colloidal suspensions and for investigating their molecular states. Components with low molecular mobility (e.g., solid contents) are difficult to detect using ^{1}H NMR, because the signals derived from solids are intensely broadened by the strong homonuclear dipolar interactions between protons. In contrast, components with high molecular mobility (e.g., dissolved molecules) provide sharp and well-resolved ^{1}H NMR spectral signals, because the dipolar interactions are averaged out by the fast motion of the molecules. Hence, it is possible to quantify a component with varied molecular mobility in a solvent by comparing its ^{1}H NMR spectrum with that of another solvent, in which the component can be completely dissolved. Thevenot et al.[43] successfully used ^{1}H NMR spectroscopy to estimate the abundance of highly mobile PEG chains on the surfaces of lipid-layer-coated poly(lactic acid) nanoparticles, by comparing the amounts of detectable PEG in the ^{1}H NMR spectra obtained from D_2O and $CDCl_3$. Here, we used D_2O and CD_3OD as solvents for ^{1}H NMR measurements, to investigate the molecular mobility of PEG on the surfaces of the ASC-DP nanoparticles (Figure 4). The results calculated using the ^{1}H NMR spectra are presented in Table 1. The compositions of the nanoparticles, which were also determined using ^{1}H NMR spectroscopy (Supporting Information S2), are listed in Table 1 as well. The molar ratios of the ASC-DP/PEGylated lipid for the rod-like ASC-DP/DSPE-PEG2000 and tube-like ASC-DP/Chol-PEG1500 nanoparticles were 66:1 and 23:1, respectively, which were significantly higher than their preparation ratio of 10:1. The nanoparticles were mainly composed of ASC-DP, with a low PEGylated lipid content. Notably, the PEGylated lipid content for the tube-like ASC-DP/Chol-PEG1500 nanoparticles was considerably higher than that for the rod-like ASC-DP/DSPE-PEG2000 nanoparticles, which could be owing to the presence of an inner tunnel surface. The

percentages of mobile PEG in the rod-like ASC-DP/DSPE-PEG2000 and tube-like ASC-DP/Chol-PEG1500 nanoparticles were approximately 94% and 65%, respectively. This indicates that most of the PEG chains in the rod-like ASC-DP/DSPE-PEG2000 nanoparticles were highly mobile, whereas the mobility of a portion of the PEG chains in the tube-like ASC-DP/Chol-PEG1500 nanoparticles was restricted. The PEG chains in the rod-like ASC-DP/DSPE-PEG2000 nanoparticles were present on the outer surface of the nanoparticles, and thus exhibited high mobility.[44] On the contrary, the tube-like ASC-DP/Chol-PEG1500 nanoparticles had an additional inner surface, where the PEG chains exhibited much lower mobility compared with those on the outer surface, owing to the nanoconfinement effect.[45]

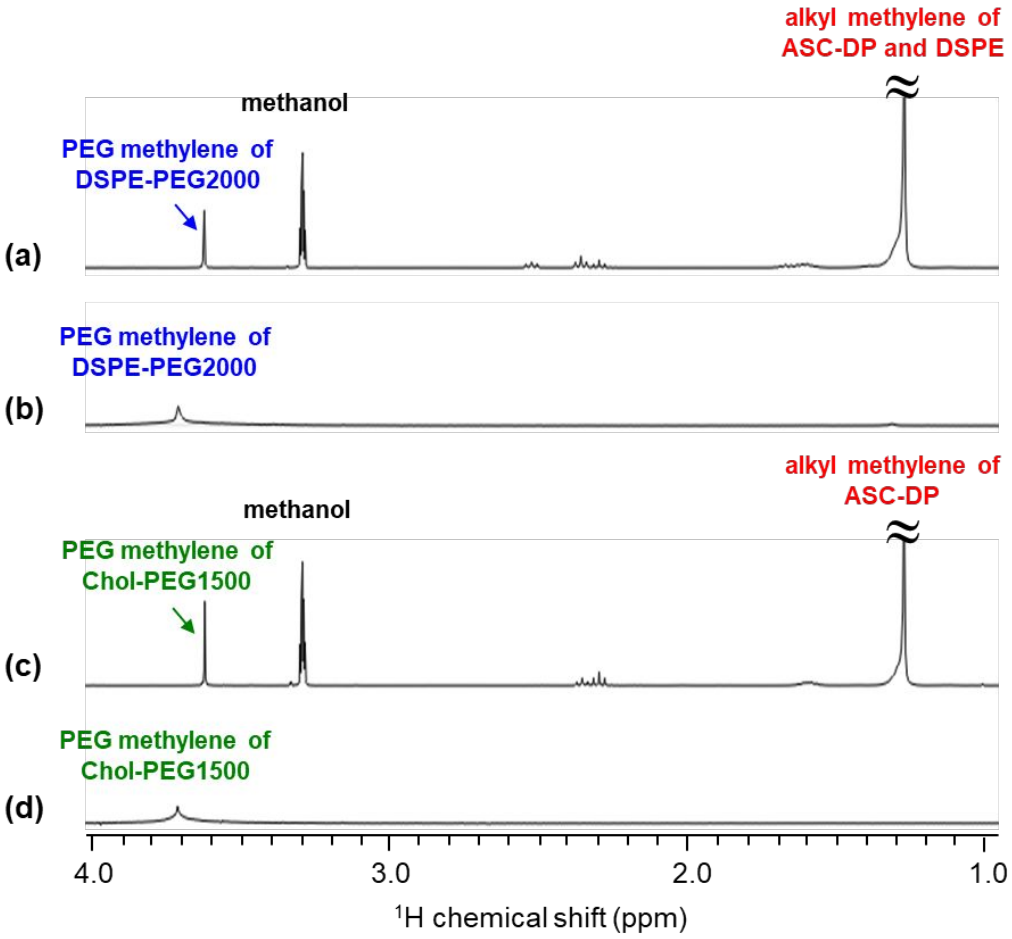

Figure 4. ^{1}H NMR spectra of (a, b) ASC-DP/DSPE-PEG2000 and (c, d) ASC-DP/Chol-

PEG1500 nanoparticles prepared at the molar ratio of 10:1 in (a, c) CD_3OD and (b, d) D_2O.

Table 1. Component compositions and percentages of mobile PEGs, for the ASC-DP/DSPE-PEG2000 and ASC-DP/Chol-PEG1500 nanoparticles prepared at the molar ratio of 10:1. All data were determined by ^1H NMR spectroscopy (n = 3, mean ± S.D.).

	Molar ratio of ASC-DP/PEGylated lipid	Mobile PEG/Total PEG, %
ASC-DP/DSPE-PEG2000	66.4 ± 4.3	94.3 ± 3.5
ASC-DP/Chol-PEG1500	22.9 ± 1.9	65.1 ± 1.1

Evaluation of the nanoparticles' internal structure

The internal structures of the rod-like ASC-DP/DSPE-PEG2000 and tube-like ASC-DP/Chol-PEG1500 nanoparticles were investigated using XRD. As shown in Figure 5, both the rod-like ASC-DP/DSPE-PEG2000 and tube-like ASC-DP/Chol-PEG1500 nanoparticles exhibited XRD patterns with diffraction peaks at 2θ = 2.3, 4.6, and 6.8º, indicating that they have similar internal structures. XRD follows Bragg's law[46] $n\lambda = 2dsin\theta$, where n is the diffraction order, λ is the wavelength of the X-rays, θ is the angle of incidence and reflection, and d is the spacing between the diffraction layers. The three observed diffraction peaks corresponded to the d-spacings of 3.8, 1.9, and 1.3 nm, respectively, and were in an approximate ratio of 1:(1/2):(1/3). This suggested a lamellar-repeated structure with an interlamellar distance of approximately 3.8 nm. Indeed, our previous SAXS study demonstrated that ASC-DP in rod-like ASC-DP/DSPE-PEG2000 nanoparticles was packed in a tilted arrangement and formed repeated bilayers with intervals of 3.7 nm, whereas DSPE-

PEG2000 was present on the particles' surfaces, yielding PEG shells that stabilized the nanoparticles (Figure 5a, inset).[35] The broad peaks observed in the 2θ range of 19–24º also demonstrated the chain sublattice in the lamellar phases of ASC-DP.[47] The tube-like ASC-DP/Chol-PEG1500 nanoparticles could exhibit the same ASC-DP packing in their internal structures, except that the innermost layer was composed of ASC-DP and Chol-PEG1500, forming an inner tunnel surface (Figure 5b, inset).

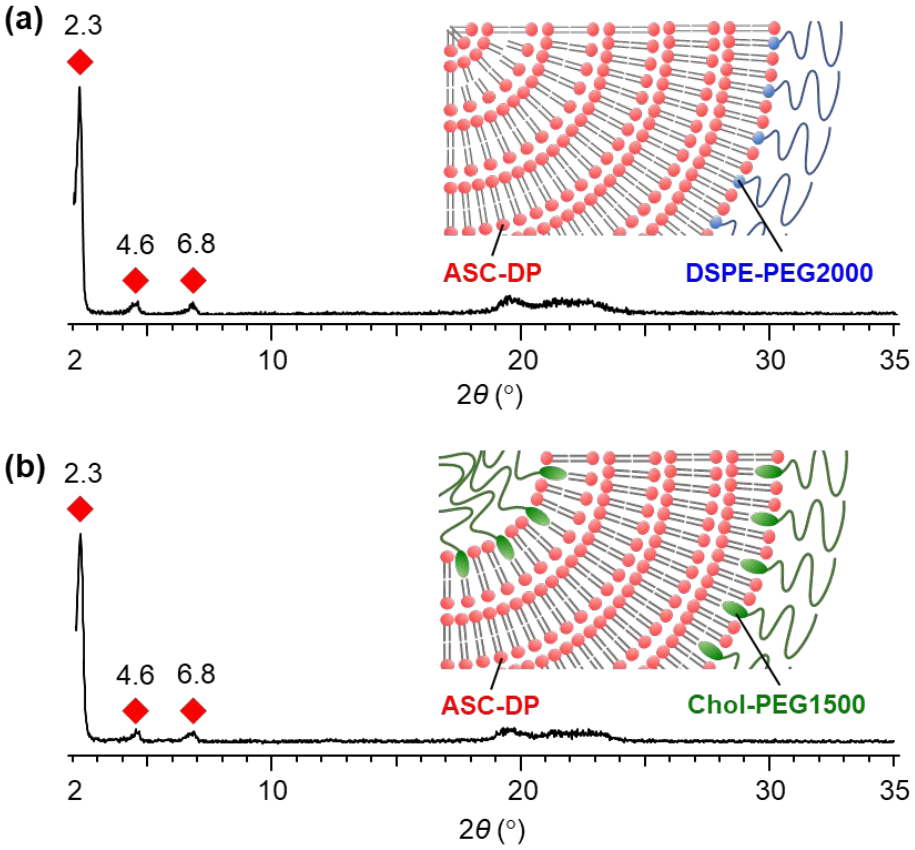

Figure 5. XRD patterns and internal structures of (a) ASC-DP/DSPE-PEG2000 and (b) ASC-DP/Chol-PEG1500 nanoparticles prepared at the molar ratio of 10:1.

Effect of the PEG molecular weight on the nanoparticles' structure

We varied the PEG molecular weight of the PEGylated lipids (PEG750 and PEG5000 for DSPE-PEG, and PEG600 and PEG4600 for Chol-PEG) and evaluated the formation of nanoparticles at different molar ratios. A similar trend, from an increase to a decrease in the particle size with increasing molar ratio, was observed for all samples (Supporting Information S4). The nanoparticles prepared at the molar ratio of 10:1 were used for further investigations. The FE-TEM images of the nanoparticles are shown in Figure 6. Nanoparticles prepared with DSPE-PEG2000 and Chol-PEG1500 at the molar ratio of 10:1 are shown for comparison. For the ASC-DP/DSPE-PEG systems, rod-like nanoparticles were obtained for all PEG molecular weights (Figure 6a-c). In contrast, tube-like nanoparticles were obtained for the ASC-DP/Chol-PEG600 and ASC-DP/Chol-PEG1500 systems (Figure 6d, e), whereas the ASC-DP/Chol-PEG4600 system exhibited rod-like nanoparticles (Figure 6f). The sizes of the nanoparticles were estimated (Table 2). The long and short axes of the nanoparticles increased with increasing PEG molecular weight, for both the ASC-DP/DSPE-PEG and ASC-DP/Chol-PEG systems. The diameters of the inner tunnel for the tube-like ASC-DP/Chol-PEG600 and ASC-DP/Chol-PEG1500 nanoparticles were 11.4 and 7.2 nm, respectively, and no tunnel space was observed for the ASC-DP/Chol-PEG4600 nanoparticles. This result suggests that the formation of the inner tunnel was strongly affected by the PEG molecular weight of Chol-PEG. Lower molecular-weight PEG was more conducive to the formation of tube-like structures.

The composition of the nanoparticles was determined by ^{1}H NMR spectroscopy (Supporting Information S2). The results are shown in Figure 7. At low PEG molecular weights (PEG750 and PEG600), the ASC-DP/Chol-PEG600 nanoparticles exhibited a higher PEGylated lipid content (i.e., a lower molar ratio of the ASC-DP/PEGylated lipid) than the ASC-DP/DSPE-

PEG750 nanoparticles. Similar to the mid-sized PEG systems (ASC-DP/DSPE-PEG2000 and ASC-DP/Chol-PEG1500), as discussed above, a significant amount of PEGylated lipid could be involved in the inner tunnel surface of the tube-like ASC-DP/Chol-PEG600 nanoparticles, leading to a higher PEGylated lipid content than for the rod-like ASC-DP/DSPE-PEG750 nanoparticles. At high PEG molecular weights (PEG5000 and PEG4600), the compositions of the two systems were not significantly different (122:1 for ASC-DP/DSPE-PEG5000 and 102:1 for ASC-DP/Chol-PEG4600), because both systems exhibited non-tunneled rod-like nanoparticles. For both the ASC-DP/DSPE-PEG and ASC-DP/Chol-PEG systems, the molar ratio of the ASC-DP/PEGylated lipid in the nanoparticles increased with increasing PEG molecular weight. PEGylated lipids were only present on the surfaces of the nanoparticles. In other words, the fraction of the PEGylated lipid on the surface layer decreased when PEGylated lipids with longer PEG chains were used. In addition, all ASC-DP/DSPE-PEG and ASC-DP/Chol-PEG nanoparticles had the same internal structures, composed of repeated ASC-DP bilayers, as they exhibited XRD patterns similar to those in Figure 5 (Supporting Information S5).

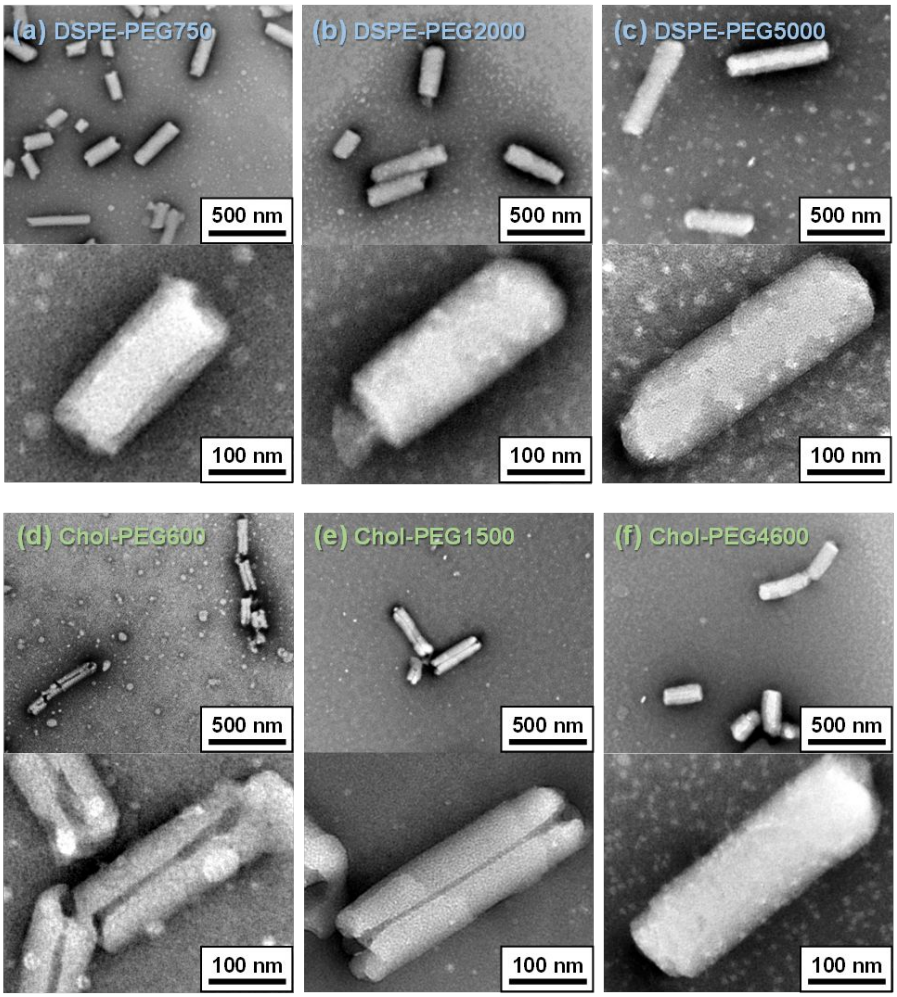

Figure 6. FE-TEM images of (a-c) ASC-DP/DSPE-PEG and (d-f) ASC-DP/Chol-PEG nanoparticles prepared at the molar ratio of 10:1. The PEG molecular weights of DSPE-PEG used for preparing the nanoparticles were (a) PEG750, (b) PEG2000, and (c) PEG5000, and those of Chol-PEG were (d) PEG600, (e) PEG1500, and (f) PEG4600, respectively.

Table 2. Mean particle sizes of ASC-DP/PEGylated lipid nanoparticles determined from FE-TEM images (n = 100, mean ± S.D.).

		Mean length, nm		
		Long axis	Short axis	Inner diameter
ASC-DP/DSPE-PEG	PEG750	250.7 ± 71.2	113.6 ± 18.1	-

	PEG2000	313.9 ± 87.8	116.1 ± 21.0	-
	PEG5000	350.8 ± 106.7	120.1 ± 20.6	-
ASC-DP/Chol-PEG	PEG600	210.3 ± 102.1	91.7 ± 19.3	11.4 ± 3.0
	PEG1500	245.6 ± 82.4	104.1 ± 15.6	7.2 ± 1.8
	PEG4600	340.2 ± 100.6	133.5 ± 28.2	-

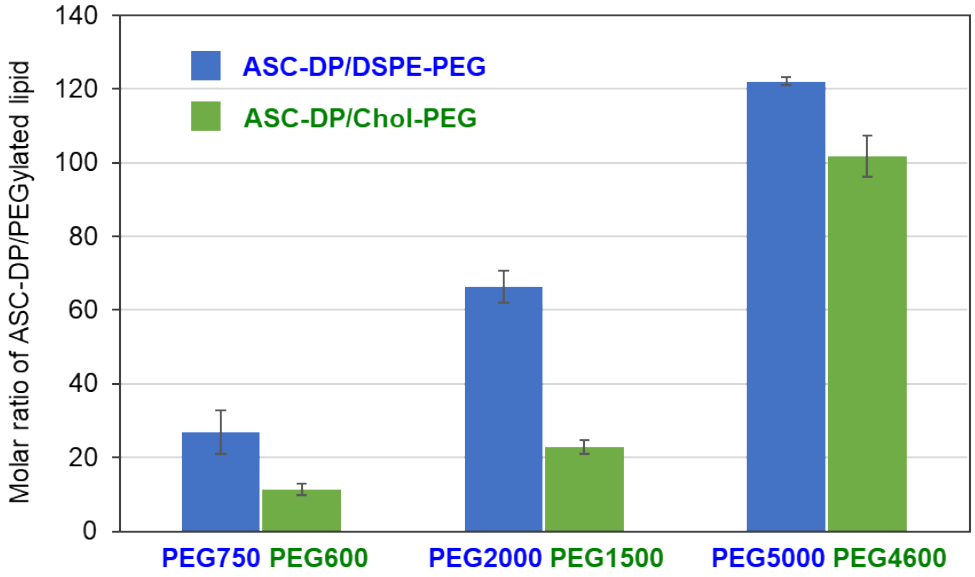

Figure 7. Component composition of ASC-DP/PEGylated lipid nanoparticles prepared at the molar ratio of 10:1. All data were determined using ^{1}H NMR spectroscopy (n = 3, mean ± S.D.).

Morphology and structure control strategy for nanoparticles

We propose a strategy to control the morphology and structure of self-assembled ASC-DP nanoparticles using PEGylated lipids, DSPE-PEG, and Chol-PEG. At higher preparation molar ratios of ASC-DP/PEGylated lipids, the nanoparticles' size decreases with increasing the preparation molar ratio. As demonstrated in our previous report, an increase in the preparation

molar ratio of ASC-DP/DSPE-PEG2000 decreased the rod-like nanoparticles' length. A higher preparation molar ratio of ASC-DP/PEGylated lipids should be more favorable for obtaining smaller-size uniform cylindrical nanoparticles. At the preparation molar ratio of 10:1, the ASC-DP/DSPE-PEG system only yielded rod-like nanoparticles (Figure 8a), whereas the ASC-DP/Chol-PEG system yielded uniform tube-like nanoparticles (Figure 8b). The nanoparticles' size, including the length and outer diameter of the cylinder, was affected by the PEG molecular weight of the PEGylated lipid. Higher PEG molecular weights yielded slightly larger nanoparticles. Therefore, in addition to the preparation molar ratio of the ASC-DP/PEGylated lipid, the PEG molecular weight allows to control the particle size. Noticeably, the inner tunnel diameter of the tube-like ASC-DP/Chol-PEG nanoparticles sensitively depended on the PEG molecular weight of Chol-PEG. As the PEG molecular weight increased, the inner tunnel gradually narrowed and ultimately disappeared (Figure 8b). Hence, the tunnel size can be modulated by altering the PEG molecular weight of Chol-PEG.

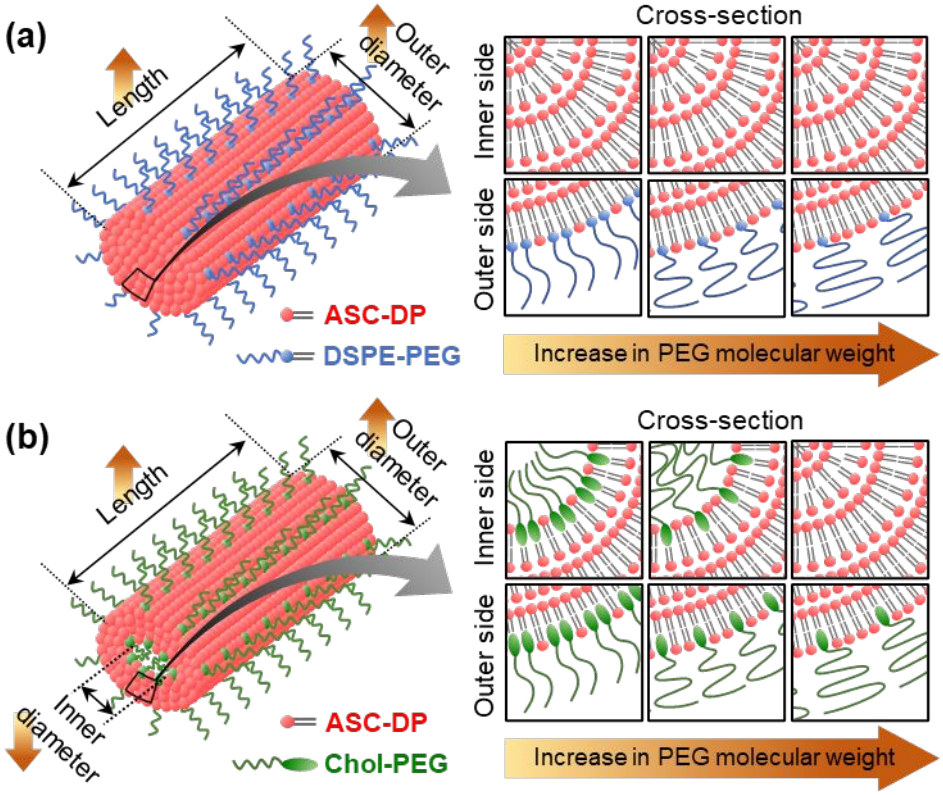

Figure 8. Morphology and structure control strategy for self-assembled ASC-DP cylindrical nanoparticles prepared with (a) DSPE-PEG and (b) Chol-PEG, at the ASC-DP/PEGylated lipid preparation ratio of 10:1.

Discussion on the rod-to-tube transformation mechanism

Here, we discuss how PEGylated lipids affect the nanostructure formation and drive the rod-to-tube transformation. The nanostructure formation is a consequence of the thermodynamic equilibrium of self-assembly. The introduction of cholesterol, which is the lipid part of Chol-PEG, into lipid monolayers resulted in the negative values of the excess Gibbs energy of mixing (ΔG_{exc}), and therefore afforded higher thermodynamic stability compared with single-component systems.[48] The most negative values of ΔG_{exc} (the most stable systems) occurred at the cholesterol molar fractions ranging from 0.25 to 0.5, depending on the lipid species.

Moreover, Kowalska et al.[49] reported that the incorporation of DSPE-PEG into a dipalmitoylphosphatidylcholine (DPPC) lipid monolayer also caused negative ΔG_{exc} values. The system with the shortest PEG chains exhibited the most negative value of ΔG_{exc}, because short PEG chains can approach DPPC molecules at much shorter distances and create fewer repulsive interactions between them, giving the system higher thermodynamic stability. We posit that the formation of the inner tunnel in the present study was owing to a balance between a reduction in the free energy caused by the mixing of multiple lipids and an increase in the free energy owing to the PEG chain repulsion (Figure 9a). The mixing of PEGylated lipids and ASC-DP on the surface layer yielded a lower energy state than that of the pure ASC-DP layers. Because the most thermodynamically stable state of the layers containing multiple lipids occurs at an intermediate mixing ratio, a significant amount of PEGylated lipids should be involved in the surface layer to achieve the most thermodynamically stable state. However, the PEG chains of the PEGylated lipids on the surface repel each other, which in turn lowers the system's thermodynamic stability. When a layer containing PEGylated lipids is bent inward, the repulsion between the PEG chains significantly increases, hindering the formation of the inner tunnel. Longer PEG chains create even stronger repulsive interactions. Therefore, in situations with high PEG-molecular-weight PEGylated lipids, tube-like structures cannot appear.

In addition, the composition of the multiple lipid layers determines the layer properties and, in turn, affects the formation of the inner tunnel surface. Specific to the ASC-DP/DSPE-PEG systems, because of the similar lipid structures of ASC-DP and DSPE-PEG, the ASC-DP layer containing DSPE-PEG may have a low toughness similar to that of the single-component lipid membranes.[41] As shown in Figure 9b, the membrane layer is not sufficiently tough to form an inner tunnel surface for the ASC-DP/DSPE-PEG system at the preparation ratio of 10:1, where

the DSPE-PEG fraction is inadequate to achieve a thermodynamically stable inner tunnel surface. Nevertheless, for the ASC-DP/Chol-PEG system, the presence of cholesterol significantly improves the toughness of the membrane layer.[41] This allows the membrane layer to be bent inward without failure, to form an inner tunnel surface, even at the relatively high preparation ratio of 10:1. Notably, shorter PEG chains are more conducive to flatter surfaces (smaller surface curvature). This is probably because more cholesterol molecules are incorporated into the ACS-DP layer when using low PEG-molecular-weight Chol-PEG, significantly increasing the area expansion modulus of the inner surface layer.[41] That is, an increase in the cholesterol fraction may lower the deformability of the inner surface layer, and therefore widen the inner tunnel.

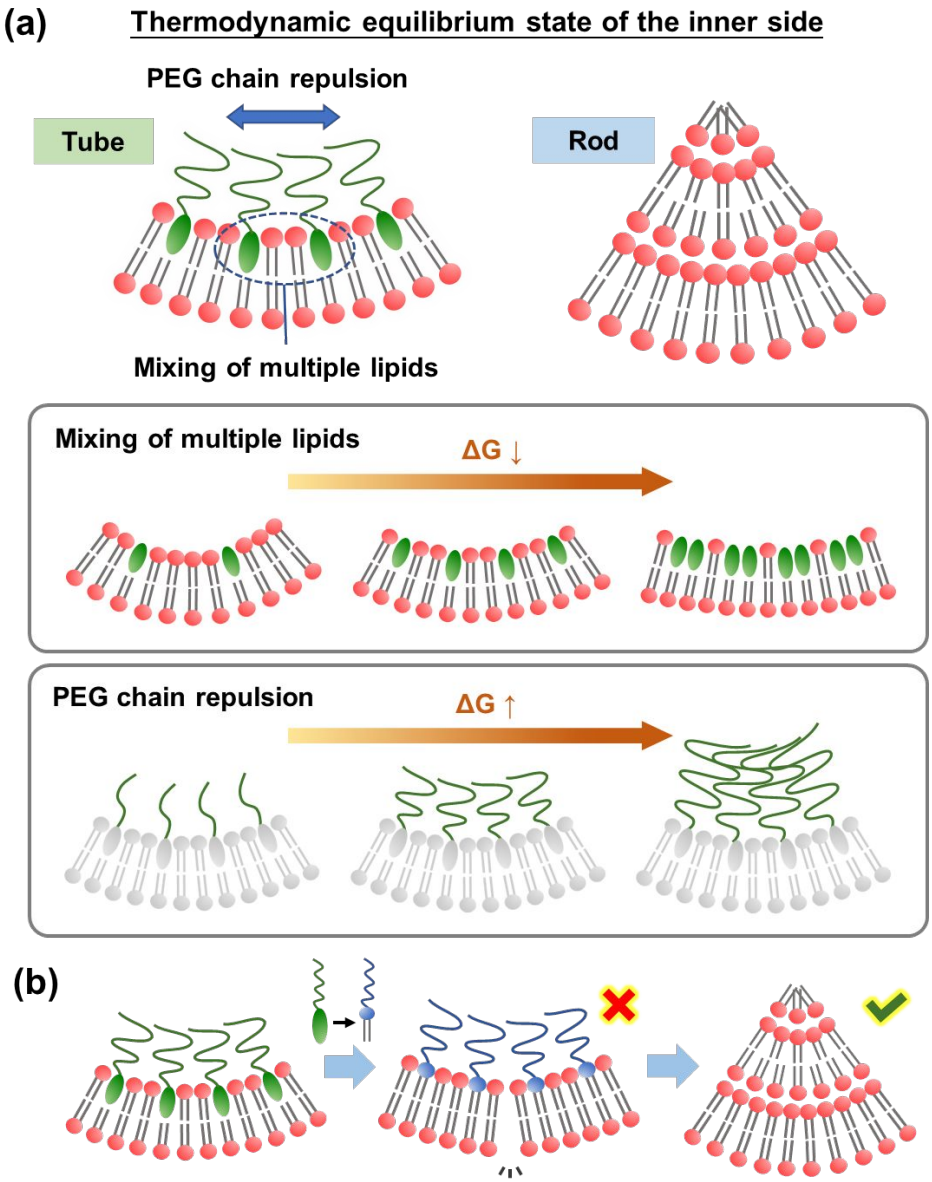

Figure 9. (a) Schematic of the tube-like and rod-like nanostructure formation as a consequence of the thermodynamic equilibrium of self-assembly, modeled for the ASC-DP/Chol-PEG system. (b) The rod-like structure formation in the ASC-DP/DSPE-PEG system at the preparation ratio of 10:1.

CONCLUSIONS

A rod-to-tube morphology control strategy for self-assembled ASC-DP cylindrical nanoparticles was successfully proposed by evaluating the effects of PEGylated lipid species

(DSPE-PEG and Chol-PEG) and PEG chain length on the formation of nanoparticles. At the preparation molar ratio of 10:1 (ASC-DP/PEGylated lipid), rod-like and tube-like nanoparticles were obtained in the ASC-DP/DSPE-PEG and ASC-DP/Chol-PEG systems, respectively. For both systems, the particle size was associated with the PEG molecular weight of the PEGylated lipid. Furthermore, the inner tunnel size of the tube-like ASC-DP/Chol-PEG nanoparticles was sensitive to the PEG molecular weight of Chol-PEG. Therefore, the rod-to-tube morphology of self-assembled ASC-DP nanoparticles can be controlled by altering the structure of the PEGylated lipid, including the lipid species and PEG chain length. We also proposed a mechanism for the rod-to-tube transformation, in which the thermodynamic equilibrium of the self-assembly was discussed. Previously, we successfully loaded hydrophobic drugs such as amphotericin B onto the disk-like ASC-DP/DSPE-PEG2000 nanoparticles prepared at a molar ratio of 1:1 and demonstrated that these nanoparticles are promising DDSs for hydrophobic drugs.[36, 37] The ASC-DP cylindrical nanoparticles reported in this study may have better drug-loading performance compared with the disk-like nanoparticles. Therefore, apart from high-dose ascorbic acid treatment, other antitumor agents could be loaded onto these nanoparticles to achieve combination therapy. The proposed morphology control strategy can guide the design of nanoparticles with better therapeutic performance. We highlight the importance of the nanoparticle form of ascorbic acid for antitumor therapy and expect that effective ascorbic acid antitumor therapy will be developed in the near future.

CONFLICTS OF INTEREST

There are no conflicts to declare.

ACKNOWLEDGMENTS

This study was supported, in part, by grants from the JSPS KAKENHI Grant-in-Aid for Scientific Research (C) (No. 16K08190 and 18K06592) and a fellowship from JST SPRING (Grant Number JPMJSP2109).

REFERENCES

1. A. T. Diplock, *Am. J. Clin. Nutr.*, 1991, **53**, 189S-193S.
2. M. P. Lupo, *Clin. Dermatol.*, 2001, **19**, 467-473.
3. J. C. Bauernfeind and D. M. Pinkert, in *Advances in Food Research*, eds. C. O. Chichester, E. M. Mrak and G. F. Stewart, Academic Press, 1970, vol. 18, pp. 219-315.
4. B. Ngo, J. M. Van Riper, L. C. Cantley and J. Yun, *Nat. Rev. Cancer*, 2019, **19**, 271-282.
5. A. Magrì, G. Germano, A. Lorenzato, S. Lamba, R. Chilà, M. Montone, V. Amodio, T. Ceruti, F. Sassi, S. Arena, S. Abrignani, M. D'Incalci, M. Zucchetti, F. Di Nicolantonio and A. Bardelli, *Sci. Transl. Med.*, 2020, **12**, eaay8707.
6. Q. Chen, M. G. Espey, M. C. Krishna, J. B. Mitchell, C. P. Corpe, G. R. Buettner, E. Shacter and M. Levine, *Proc. Natl. Acad. Sci. U. S. A.*, 2005, **102**, 13604-13609.
7. S. Pal and N. R. Jana, *ACS Appl. Nano Mater.*, 2022, **5**, 4583-4596.
8. J. Yun, E. Mullarky, C. Lu, K. N. Bosch, A. Kavalier, K. Rivera, J. Roper, I. I. C. Chio, E. G. Giannopoulou, C. Rago, A. Muley, J. M. Asara, J. Paik, O. Elemento, Z. Chen, D. J. Pappin, L. E. Dow, N. Papadopoulos, S. S. Gross and L. C. Cantley, *Science*, 2015, **350**, 1391-1396.
9. Y. Dang and J. Guan, *Smart Mater. Med.*, 2020, **1**, 10-19.
10. J. Shi, A. R. Votruba, O. C. Farokhzad and R. Langer, *Nano Lett.*, 2010, **10**, 3223-3230.
11. A. Chakraborty and N. R. Jana, *ACS Appl. Mater. Interfaces*, 2017, **9**, 41807-41817.
12. S. K. Golombek, J.-N. May, B. Theek, L. Appold, N. Drude, F. Kiessling and T. Lammers, *Adv. Drug Deliv. Rev.*, 2018, **130**, 17-38.
13. O. C. Farokhzad and R. Langer, *ACS Nano*, 2009, **3**, 16-20.
14. A. Albanese, P. S. Tang and W. C. Chan, *Annu. Rev. Biomed. Eng.*, 2012, **14**, 1-16.
15. P. Decuzzi, B. Godin, T. Tanaka, S.-Y. Lee, C. Chiappini, X. Liu and M. Ferrari, *J. Control. Release*, 2010, **141**, 320-327.
16. S. Barua, J.-W. Yoo, P. Kolhar, A. Wakankar, Y. R. Gokarn and S. Mitragotri, *Proc. Natl. Acad. Sci. U. S. A.*, 2013, **110**, 3270-3275.
17. Y. Guo, L. Xu, H. Liu, Y. Li, C.-M. Che and Y. Li, *Adv. Mater.*, 2015, **27**, 985-1013.
18. S. Zhang, *Nat. Biotechnol.*, 2003, **21**, 1171-1178.
19. L. C. Palmer and S. I. Stupp, *Acc. Chem. Res.*, 2008, **41**, 1674-1684.

20. G. M. Whitesides, J. P. Mathias and C. T. Seto, *Science*, 1991, **254**, 1312-1319.
21. C. V. Kulkarni, *Nanoscale*, 2012, **4**, 5779-5791.
22. T. Shimizu, H. Minamikawa, M. Kogiso, M. Aoyagi, N. Kameta, W. Ding and M. Masuda, *Polym. J.*, 2014, **46**, 831-858.
23. T. G. Barclay, K. Constantopoulos and J. Matisons, *Chem. Rev.*, 2014, **114**, 10217-10291.
24. T. Shimizu, *J. Polym. Sci. A: Polym. Chem.*, 2006, **44**, 5137-5152.
25. C. H. Kim, S. G. Lee, M. J. Kang, S. Lee and Y. W. Choi, *J. Pharm. Investig.*, 2017, **47**, 203-227.
26. M. Liu, J. Li, D. Zhao, N. Yan, H. Zhang, M. Liu, X. Tang, Y. Hu, J. Ding, N. Zhang, X. Liu, Y. Deng, Y. Song and X. Zhao, *Biomaterials*, 2022, **283**, 121415.
27. Z. Chen, K. Higashi, K. Ueda and K. Moribe, *Mol. Pharm.*, 2022, **19**, 188-199.
28. Y. Hasegawa, K. Higashi, K. Yamamoto and K. Moribe, *Mol. Pharm.*, 2015, **12**, 1564-1572.
29. H. Zhou, Z. Fan, P. Y. Li, J. Deng, D. C. Arhontoulis, C. Y. Li, W. B. Bowne and H. Cheng, *ACS Nano*, 2018, **12**, 10130-10141.
30. N. B. Shah, G. M. Vercellotti, J. G. White, A. Fegan, C. R. Wagner and J. C. Bischof, *Mol. Pharm.*, 2012, **9**, 2146-2155.
31. C. D. Walkey, J. B. Olsen, H. Guo, A. Emili and W. C. W. Chan, *J. Am. Chem. Soc.*, 2012, **134**, 2139-2147.
32. J. L. Perry, K. G. Reuter, M. P. Kai, K. P. Herlihy, S. W. Jones, J. C. Luft, M. Napier, J. E. Bear and J. M. DeSimone, *Nano Lett.*, 2012, **12**, 5304-5310.
33. M. Li, S. Jiang, J. Simon, D. Paßlick, M.-L. Frey, M. Wagner, V. Mailänder, D. Crespy and K. Landfester, *Nano Lett.*, 2021, **21**, 1591-1598.
34. Q. Yang, S. W. Jones, C. L. Parker, W. C. Zamboni, J. E. Bear and S. K. Lai, *Mol. Pharm.*, 2014, **11**, 1250-1258.
35. Z. Chen, K. Higashi, R. Shidara, K. Ueda, T. Morita, W. Limwikrant, K. Yamamoto and K. Moribe, *Int. J. Pharm.*, 2021, **602**, 120599.
36. K. Higashi, F. Mibu, K. Saito, W. Limwikrant, K. Yamamoto and K. Moribe, *Eur. J. Pharm. Sci.*, 2017, **99**, 24-31.
37. K. Moribe, S. Maruyama, Y. Inoue, T. Suzuki, T. Fukami, K. Tomono, K. Higashi, Y. Tozuka and K. Yamamoto, *Int. J. Pharm.*, 2010, **387**, 236-243.
38. V. S. Saji, *Mater. Today Adv.*, 2022, **14**, 100239.
39. T. Shimizu, W. Ding and N. Kameta, *Chem. Rev.*, 2020, **120**, 2347-2407.
40. C. Kirby, J. Clarke and G. Gregoriadis, *Biochem. J.*, 1980, **186**, 591-598.
41. D. Needham and R. S. Nunn, *Biophys. J.*, 1990, **58**, 997-1009.
42. H. Xu, K. Q. Wang, Y. H. Deng and D. W. Chen, *Biomaterials*, 2010, **31**, 4757-4763.
43. J. Thevenot, A.-L. Troutier, L. David, T. Delair and C. Ladavière, *Biomacromolecules*, 2007, **8**, 3651-3660.
44. K. Abe, K. Higashi, K. Watabe, A. Kobayashi, W. Limwikrant, K. Yamamoto and K. Moribe, *Colloids Surf. A Physicochem. Eng. Asp.*, 2015, **474**, 63-70.
45. I. De Santo, F. Causa and P. A. Netti, *Anal. Chem.*, 2010, **82**, 997-1005.
46. W. H. Bragg, *Proc. R. Soc. Lond. A*, 1913, **89**, 246-248.
47. D. Marsh, *Chem. Phys. Lipids*, 2012, **165**, 59-76.
48. M. Jurak, *J. Phys. Chem. B*, 2013, **117**, 3496-3502.

49.M. Kowalska, M. Broniatowski, M. Mach, Ł. Płachta and P. Wydro, *J. Mol. Liq.*, 2021, **335**, 116529.